Migration of tremor locations before the 2008 eruption of Meakandake Volcano, Hokkaido, Japan

Masashi Ogiso[a,1,*], Kiyoshi Yomogida[b]

[a] *Sapporo District Meteorological Observatory, Sapporo, 060-0002, Japan*
[b] *Earth and Planetary Dynamics, Graduate School of Science, Hokkaido University, Sapporo, 060-0810, Japan*

Abstract

We estimate the locations of three tremor sequences, denoted A, B, and C, that occurred before the 2008 eruption at Meakandake volcano, eastern Hokkaido, Japan, using the spatial distribution of seismic amplitudes of volcanic tremor. Although we used only five seismic stations, we could estimate the location of three tremor sequences. We find two source areas. The location area of tremor A is about 2 km southwest of the erupted crater (area a) and the other about 1 km southeast to south of the crater as that of the tremor B (area b). For the tremor B, the location of its early phase is estimated in area a while the location of its later phase appears to connect the area a and b. This location migration of tremor B occurred simultaneously with other important geophysical phenomena before the eruption event. Our findings of two location areas of tremor sequences and location migration

*Corresponding author
[1] Now at Osaka District Meteorological Observatory, Osaka, 540-0008, Japan

of tremor B are important for monitoring activities at Meakandake volcano, particularly the location of a possible phreatic eruption.

Keywords: tremor location, migration, phreatic eruption, Meakandake

1. Introduction

Volcanic tremor is one of the most important phenomena to interpret on-going volcano activity. Tremor generally occurs when volcano activity is enhanced. Despite its significance, tremor location is rarely estimated, because phase arrivals of tremor are not clear in most cases, so that conventional hypocenter determination approaches cannot be applied directly. Recently, with the improvement of portable seismometers, broadband seismic observation around active volcanoes has been widely conducted. Analysis of long-period (LP) or very long-period (VLP) signals including volcanic tremor reveal not only location but also source mechanism of such events. On the other hand, seismic array is another powerful tool to estimate tremor locations. Instead of reading phase arrivals, correlation among waveform records is used in array analysis (e.g. Kawakatsu and Yamamoto, 2007). These two techniques require special equipments, that is, broadband seismometers and seismic array composed of many adjacent stations, respectively. In most cases of active volcanoes, however, seismic observation networks are consti-

tuted by only a very limited number of short-period seismometers that can be used only for locating earthquakes with clear phase arrivals.

New approaches for tremor location determination have been recently proposed even with a small number of stations of short-period seismometers. Battaglia and Aki (2003) estimated locations of volcanic earthquakes and tremor at Piton de la Fournaise, an active volcano in Reunion Island, using the spatial distribution of seismic wave amplitudes. Their basic idea is the same as an old study of Yamasato (1997) or Jolly et al. (2002) who estimated the source location of pyroclastic flows. Kumagai et al. (2010) revealed that the method of Yamasato (1997), Jolly et al. (2002) and Battaglia and Aki (2003) are based on the characteristics of intensive scattering of seismic waves in volcanic areas, and the location method of seismic events is useful to monitor volcanic activities even if there are a limited number of seismic stations. This location method does not need special equipments and appears to be applied to a conventional seismic network with short-period seismometers in most of active volcanoes.

Meakandake volcano, located in an eastern part of Hokkaido, Japan, is one of the volcanoes that erupt repeatedly at present in Japan. On November 18 and 28, 2008, small phreatic eruptions occurred at Meakandake. Before

and associated with the eruption activity, significant seismicity and tremor activity were observed. In this study, we estimate the locations of tremor sequences that occurred during the eruption activities of Meakandake in 2008, using the location method of Battaglia and Aki (2003) or Kumagai et al. (2010). We then discuss the relationship of the estimated tremor locations and the observed eruption activity on the surface.

2. Eruption sequences of Meakandake in 2008

In this section, we shall introduce the overall features of Meakandake volcano and its 2008 eruption sequence.

There are three main craters on Meakandake volcanic body, called Pon-machineshiri, Naka-machineshiri and Akanfuji, as shown in Fig. 1. The latest intensive magmatic eruption at Meakandake volcano occurred about 1000 years ago. All of the eruptive activities of Meakandake volcano recorded since 1954 were phreatic eruptions at either Pon-machineshiri and Naka-machineshiri (Japan Meteorological Agency, 2005). Especially, recent eruptions starting in 1988 occurred at a southeastern side of Pon-machineshiri, except for the 2006 eruption which occurred at its northwestern side.

Starting in the end of September 2008, seismic activities were intensi-

fied at Meakandake (Fig. 2). On November 18, substantial ash fall around the 96-1 crater, located in the southeastern side of Pon-machineshiri, was observed by Volcanic Observations and Information Center, Sapporo District Meteorological Observatory (hearafter Sapporo VOIC), recognizing it as the eruption of Meakandake in an official manner. Subsequently, gray plume from the 96-1 crater was observed from November 28 to 29, as intensive volcanic activity continued. All the eruptions in November 2008 were phreatic with the amount of ash flows estimated about 12,000 tons in total (Ishimaru et al., 2009). During these eruption activities, no significant visual changes were observed around the 2006 craters located in a northwestern side of Pon-machineshiri (Sapporo VOIC, 2008). Figure 3 shows the hypocentral distribution at Meakandake volcano from July to December 2008. A focal area of seismic swarms starting in September was around the 96-1 crater, in the southeastern side of Pon-machineshiri. No significant horizontal migrations of hypocenters were observed before eruptions in November. After these eruptions, hypocenters became slightly shallower than those before them.

Some sequences of tremor occurred during the 2008 activities of Meakandake (Fig. 2). During the first seismic swarm in the end of September, the first clear tremor with the duration time of 4 minutes occurred on September

29. The maximum amplitude of this tremor at station V.MEAB is 2.4μm, which is the largest tremor amplitude during the entire 2008 activity. Seismicity became high after this tremor, as shown in Fig. 2. Daily frequency of earthquakes was 788 on September 29, which is also the largest during the 2008 activity. Hypocenters of earthquakes did not change clearly before and after this tremor (Fig. 3). We call it tremor A. Two days before the eruption on November 18, tremor with the duration time of 30 minutes occurred on November 16. Seismic activity did not enhance before and after the occurrence of this tremor. After this tremor, however, some continuous tremor sequences with low amplitude and long duration time occurred frequently. Especially, the tremor began at 3:37 on November 18 had the longest duration time of 36 hours. A small eruption is inferrd to have occurred during this tremor sequences (Ishimaru et al., 2009). We call the tremor that occurred on November 16 as tremor B, and the latter continuous tremor as tremor C.

In this study, we estimate the locations of the above three characteristic tremors A, B, and C, using the spatial distribution of tremor amplitudes (Battaglia and Aki, 2003; Kumagai et al., 2010). These three tremors are important, because they appeared to be closely related to the intensive seismic activity and the eruptions.

3. Method of estimation of tremor location

In this section, we summarize the method of locating tremor with the spatial distribution of its seismic amplitudes (Battaglia and Aki, 2003; Kumagai et al., 2010). Assuming body waves in a waveform record, seismic amplitude of the band limited seismogram around frequency f at the i-th station, $A_i(f)$, is expressed in the frequency domain as follows;

$$A_i(f) = A_0 \cdot \frac{\exp(-Br_i)}{r_i} \cdot S_i(f). \tag{1}$$

where A_0 is the amplitude term at the source, r_i is the distance between the source and the i-th station, $S_i(f)$ is the site amplification factor at the i-th station, and B represents the total attenuation coefficient expressed by the quality factor Q due to scattering and intrinsic attenuations and the velocity of a medium β, as follows;

$$B = \frac{\pi f}{Q\beta}. \tag{2}$$

Strictly speaking, the radiation pattern of seismic source, volcanic tremor in this case, is far from isotropic. Kumagai et al. (2011) showed that the observed radiation pattern in 5 Hz or higher frequencies is generally not noticeable, using the simulation of scattering waves with heterogeneous media

and topography, so that we may assume isotropic radiation in the present case. In contrast, the site amplification factor, $S_i(f)$, seems very variable in this frequency range, so that we need to correct it, as introduced in eq. (1).

After correcting the site amplification factor $S_i(f)$, we calculate the coefficient A_0 from the observed amplitude at the i-th station ($i = 1 \cdots N$);

$$A_0 = \frac{1}{N} \sum_{i=1}^{N} A_i r_i \exp(B r_i). \tag{3}$$

Normalized residual errors in location estimation is defined as follows;

$$Error \equiv \frac{\sum_{i=1}^{N} \{A_i - A_0 \exp(-B r_i)/r_i\}^2}{\sum_{i=1}^{N} A_i^2}. \tag{4}$$

To estimate each assigned tremor location, we would minimize the above error in eq. (4). As seen in eq. (1), we have to assume the medium velocity β and quality factor Q. Since the majority of tremor at frequency higher than 5 Hz is composed by direct S waves and scattered by structural heterogeneities along the ray path of direct S waves (Kumagai et al., 2010), we use $\beta = 1.44$ km/s in this study, same as the S wave velocity used by Sapporo VOIC for earthquake location at Meakandake. No investigations has been conducted about the estimation of Q around Meakandake. We assume Q to be constant

143 of 50, which Koyanagi et al. (1995) estimated around volcanic areas in Hawaii.

144 4. Data

145 Sapporo VOIC operates six seismic stations with seismometers with the
146 natural period of 1 s to monitor seismic activities of Meakandake volcano
147 (Fig. 1). While two stations, V.NSYM and V.PMNS, have only an UD
148 component, the other stations have three components. For the estimation of
149 tremor locations, we selected tremor waveforms from continuously recorded
150 waveforms at five stations, V.MEAA, V.MEAB, V.PMNS, V.NSYM and
151 V.MNDK (Fig. 1). Since two stations, V.NSYM and V.PMNS, have only an
152 UD component, we used this component at each record in this study. We
153 filtered tremor waveforms with a bandpass filter of 5-10 Hz ($f = 7.5$ Hz in eq.
154 1), because we may assume an isotropic radiation due to scattering effect of a
155 medium in this frequency range (Kumagai et al., 2011). Next, we calculated
156 each RMS amplitude using three time windows (20 s, 60 s, and 100 s) in the
157 duration time of the tremor. Since the radiation pattern of tremor source is
158 collapsed by structural heterogeneities along ray path, the energy of direct S
159 waves from tremor source is mainly shared in its early coda waves. Although
160 such coda waves does not radiation pattern, the energy of coda waves are

almost the same as those of direct S waves. Calculating RMS amplitude emphasize the energy of those coda waves, so it is reasonable to apply eq. (1) which is correct for direct S waves in estimation of tremor location. The spatial resolution scale that we focus is about 2 or 3 km, corresponding to the travel time of S wave to be about a few seconds in record. Although Kumagai et al. (2010) proposed that it is effective to shift the time window for RMS calculation according to the travel time from assumed source to the station, we does not shift the time windows for RMS calculation, because travel time of S wave is smaller than the time windows.

After calculating RMS amplitudes and correcting site amplification effect at five stations, we conduct a grid search in the three-dimensional space to minimize eq. (4) by changing source locations. Intervals of the grid search were 0.001 degree in horizontal directions and 0.1 km in a depth direction.

All the date and time used in this paper are based on its local time system called Japan Standard Time.

5. Estimation of site amplification factors

As explained in section 3, the correction of site amplifications is important in the present location analysis. The coda normalization method (Phillips

and Aki, 1986) has been widely applied to estimate site amplification factors. Coda waves are generally defined in the time window after twice as travel time of the S waves and are composed of backscattered waves from structural heterogeneities spread over a large area. In this case, the amplitude of coda waves depends only on its source factor and site amplification factor, because all the records show a common-value of coda Q in high frequency, including our seismic stations around Meakandake. Thus, we can estimate the relative site amplification factor of each station stably with respect to a given master station by the coda normalization method.

We estimate site factors by the coda normalization method with regional events shown in Fig. 4 because the source factor of each earthquake can be assumed common. Using the unified hypocenter catalogue of Japan Meteorological Agency and the JMA2001 travel time table (Ueno et al., 2002), we calculated the arrival time of the direct S phase in each record. Next, we selected seismic waveforms in the duration of 10.24 s after twice as the calculated S arrival as our coda window, then calculated power spectrum ratios to that of the reference station V.MEAB in which the absolute site effect seem to be minimum for all the stations. A parzen window of 0.4 Hz was applied to obtain smooth power spectrum. In an active volcano area, the

coda normalization method would not give proper site amplification factors in some cases, probably because of the existence of localized heterogeneities such as a magma chamber (Kumagai et al., 2009). In order to test this, we also calculate the power spectrum ratios of direct S waves, with 20.48 s in duration starting at 0.5 s before the predicted S arrivals, in order to check the stability of site amplification factors estimated by the coda normalization method.

Figure 5 shows each measured coda spectrum ratios in gray, and the averaged ratio in black for each station. The averaged spectrum ratio of the direct S wave is also shown in Fig. 5. In spite of all the stations located within about 3 km from the summit of Meakandake, spectral ratios vary significantly among stations. For example, V.PMNS and V.NSYM are in the similar environment (in the steep slope of a volcanic body), but the factors differ significantly from each other. While a relatively steep spectral peak between 4 and 5 Hz is seen in V.PMNS, no such peaks are found in V.NSYM. On the other hand, V.MNDK, located in the saddle of volcano peaks have no significant spectral peaks below 10 Hz, but almost twice with respect to V.MEAB. These results indicate that we have to correct site amplification effects carefully to apply the present method to estimate tremor locations.

The spectral ratios of the direct S wave and coda show almost the same features, for example, a steep spectral peak around 4 Hz at V.NSYM. This fact suggests that there would not be any scatterers distributed in a systematic manner but they are rather randomly distributed beneath Meakandake volcano, and the coda normalization method would give us proper site amplification factors.

We averaged the spectral ratio between 5 to 10 Hz of each earthquakes, then averaged among all earthquakes to obtain the site amplification factor for this study. The values of the site amplification factor and its standard deviation are shown in table 1. The amplitude of tremor sequences we analyze is large enough so we can ignore the influence of certainty of site amplification factors in eq. (3).

6. Estimation of Tremor locations

In this section, we explain the results of our location estimation for the three tremor sequences mentioned in section 2: Tremors A, B and C, using the method described in section 3.

6.1. Estimation of volcano-tectonic earthquake

First, we estimate the volcano-tectonic (VT) earthquake using the method in section 3 and compare the location with the routine location estimated by phase arrivals to check the accuracy of our location estimation.

We selected the VT earthquake occurred at 18:02 on March 23, 2009. Bandpass filtered (5-10 Hz) waveform recorded at station V.MEAB is shown in Fig. 6. Origin time and theoretical arrival times of P and S phases calculated from routine location are also shown in the figure. Small earthquake occurred just before the earthquake, bud it did not affect to phase reading and our location estimation. The time window of calculating RMS amplitude is 3 s from the appearance time of maximum amplitude. As seen in Fig. 6, the time window corresponds to the direct S wave and its early coda wave. Figure 7 shows the estimated location of this earthquake and routine location. Estimated location by the amplitude is about 1 km south and 1 km deeper than the routine location. The result means that our assumption of isotropic radiation pattern of direct S wave and its early coda wave is generally appropriate, but we have to take the difference into account to discuss the absolute location. We think that the horizontal heterogeneity of Q causes such the difference in location estimation. The low Q medium spread under

the Pon-machineshiri crater. The wave to the northern station (V.NSYM or V.MEAA) attenuate strongly than that to the southern station (V.MNDK). So the location from our method is southerly compared with that from phase arrivals.

Next, we check the influence of the value of Q with the same earthquake. Assuming three values of Q (50, 75 and 100), we conducted the location estimation. Figure 8 shows the result of location with three different Q values. The location of three Q values are almost the same, so that the values of Q does not have significant effect in this location method. So we use 50 for the value of Q, mentioned at section 3.

6.2. Tremor A on September 29

Figure 9(a) shows the waveform of tremor A at station V.MEAB. Tremor began at 14:11 (81 s in the figure) and ended at 14:15 (321 s in the figure) on September 29. We analyzed an early part between 85 and 180 s, including a part of large amplitude, because a later part seems to be contaminated by some earthquakes that occurred late. Figure 9(b) shows the power spectrum of tremor A at station V.MEAB. No significant spectral peaks are noticed, and the power of 5-10 Hz is sufficient for the present analysis. We calculated RMS amplitudes with the time window of 20 s and each window shifted by

10 s. We used the five seismic stations shown in Fig. 1. In the time of large amplitude (about 105 s to 155 s in Fig. 9a), the record of V.PMNS was off scale, so we excluded the data of this station.

Figure 10 shows the spatial distribution of errors in our location estimation defined by eq. (4) at the time window of 95 s. In a horizontal direction, the area of small errors spreads about 1 km in the NE-SW direction but less than 1 km in NW-SE. It is because the distribution of seismic stations is limited in the NW-SE direction from the possible location, as seen in Fig. 1. We may conclude that the precision of tremor locations is about 1 km in both horizontal and vertical directions.

The estimated tremor locations for analysis time window of tremor A are shown in Fig. 11. They are concentrated in the western part of Akanfuji, about 2 km southwest from the 96-1 crater. Because of the exclusion of data at V.PMNS, some locations are estimated at almost surface, although locations in the horizontal direction are estimated stably. Figure 12 shows temporal variations of RMS amplitude ratios with respect to V.PMNS. The record of V.PMNS was off scale in the shaded area. The amplitude ratio between V.NSYM and V.MEAB is almost the same during the sequence of tremor A. That is, no significant temporal changes of tremor location are

found.

Only the ray path from source area of this tremor to the station V.NSYM passes under the Pon-machineshiri crater. So the influence of horizontal heterogeneity of Q would not affect so much to the absolute location compared with the case of VT earthquake in the previous section.

6.3. Tremor B on November 16

Tremor B started at 00:56 (410 s in Fig. 13a) on November 16, then strong motions continued for about 8 minutes, followed by weak motions for about 20 minutes, as shown in Fig. 13(a) at station V.MEAB. The total duration time of tremor B was about 30 minutes. Visual observations of activities around the craters were not available because the craters were covered by cloud. Seismicity did not change noticeably before or after tremor B (Fig. 2).

We divided this tremor into three phases, phases 1, 2 and 3, based on the temporal variation of tremor amplitude, as observed, for example, at station V.MEAB (Fig. 13a). The end of phase 3 is set to be at 1440 s, because some earthquakes are overlapped after this timing. Figure 13(b) shows the power spectra of the three phases. The overall spectral shape of phase 2 is similar to that of phase 1. No significant spectral peaks are found during the three

phases of this tremor. We calculated RMS amplitudes with the time window of 60 s with each window shifted by 30 s. No seismograms are off scale during this tremor, so that we could use all the five stations for location estimation.

The distribution of location errors for the time window at 1190 s (phase 3) is shown in Fig. 14. Similar to tremor A (Fig. 10), the area of small errors tends to spread in the NE-SW direction. The precision of our tremor location is estimated to be as 1 km in both horizontal and vertical directions. Figure 15 shows the estimated tremor locations for three phases. We plot red, green and blue stars for phases 1, 2 and 3, respectively. Compared with the case of tremor A (Fig. 11), the precision in the depth direction is improved by the additional data at V.PMNS. While the locations of phase 3 are distributed from the north of Akanfuji to the south of the 96-1 crater, those of phases 1 and 2 are distributed in the NW area of Akanfuji, almost same as those of tremor A. Although errors in our location estimation spreads in the NE-SW direction (Fig. 14), the differences in locations between phase 1 or 2 and phase 3 does not be caused from the limited spatial resolution in present analysis.

Figure 16 shows RMS amplitude ratios of tremor B with respect to V.PMNS. For phases 1 and 2, the amplitude ratios of V.MEAB and V.NSYM

are almost the same. In contrast, those of V.NSYM become larger than those of V.MEAB for phase 3. Considering eq. (1), the amplitude ratio should reflect the relative distance between source and station. Nearly similar values of V.MEAB and V.NSYM mean that the sources for phases 1 and 2 are located at the same distance from V.MEAB and V.NSYM. On the other hand, the large ratio of V.NSYM implies that the distance became short from the source of phase 3 to the station V.NSYM. In addition, we show the error distribution of phase 1 and 2, and the time series of errors in Fig. 17. As seen in Fig. 17(a), (b) and Fig. 14, the peak of small error is only one among all three phases. This fact means that there may be only one source at the time. Also, Fig. 17(c) shows that the value of minimum error does not change significantly among three phases. If there are two sources of tremor, the peak of small error is broadened and the value of minimum error should become large compared with the case of one source. It is possible that tremor occurs simultaneously at two source areas, but the source where waves radiated strongly should be different between phase 1 or 2 and phase 3. Although their absolute locations cannot be estimated precisely due to the limitation of the station distribution in the present analysis, we can clearly conclude that relative locations of phases 1 and 2 should be different from those of

phase 3. In addition, the locations of phase 2 are determined deeper than those of phase 1 (Fig. 15). As seen in Fig. 16, the amplitude ratios of phase 2 at all the stations are larger than those of phase 1 in general. This fact means that the tremor source appears to have migrated downwards during the main part of tremor B, from phase 1 to phase 2.

The influence of heterogeneity of Q may not be significant at the absolute location area of phase 1 and 2, although the absolute location area of phase 3 may be northerly and shallow because of the influence of Q.

6.4. Tremor C on November 17 to 19

Figure 18 shows the continuous waveform recorded at V.MEAB from 09:00 on November 17 to 16:00 on November 19. Beginning and ending of this continuous tremor are showed in blue and red lines, respectively after the determination of Sapporo VOIC. We select the following three parts of the continuous tremor: (a) beginning at 10:15 on Nov. 17, (b) beginning at 21:04 on Nov. 17, and (c) beginning at 3:37 on Nov. 18. The power spectra of five parts of this tremor are shown in Fig. 19. All the spectra were calculated with the time window of one hour and the beginning time of window showed in the legend of Fig. 19. No spectral peaks are noticeable, and the spectral structures are similar to each other. Different from tremor A

or B, the amplitude of continuous tremor C are slowly varied. It is therefore difficult to define the beginning and ending of tremor C. We estimated tremor locations for the following three time windows: (a) from 10:30 to 12:30 on Nov. 17, (b) from 21:30 on Nov. 17 to 01:30 on Nov. 18 and (c) from 04:00 on Nov. 18 to 06:00 on Nov. 19. We selected these time windows, because the tremor signals were clearly recorded at all the five seismic stations. The time window for RMS amplitude calculations spans 100 s, with each window shifted by every 50 s. Estimated tremor locations are shown in Fig. 20. The locations spread from about 1 km south to southeast of the 96-1 crater. Location depths are distributed from 0.5 km to -0.5 km with the average of 0 km (sea level), commonly among the three tremor parts.

Fig. 21 shows the amplitude ratios with the time windows of Fig. 18 with respect to V.PMNS. Blue lines indicate the time that we estimated the location in our present analysis while not, but counted as tremor by Sapporo VOIC in black lines. The average of amplitude ratios at V.MEAA is about 0.3 and that at V.MEAB is about 0.4, which does not vary so much during the analyzed time. These features are similar to those of phase 3 of tremor B, implying that the location of tremor C is clearly different from those of tremor A and phase 1 or 2 of tremor B. The spreading of the estimated locations

385 in the NE-SW direction is probably artificial owned to the geometry of the
386 present station distribution (Fig. 1).

387 The absolute location of tremor C may be northerly and shallow because
388 of the influence of Q, so tremor C would occur just under the 96-1 crater.

389 7. Eruption Model for the 2008 event

390 In the previous sections, we revealed two source areas among the tremor
391 sequences that we analyzed. Figure 22(a) summarizes these locations. The
392 locations of tremor A and phase 1 or 2 of tremor B are at the NW part
393 of Akanfuji (area a) while tremor C are near the 96-1 crater (area b). The
394 locations of phase 3 of tremor B appear to connect these two source areas.
395 The distance between two source areas is about 1 km. In addition, the depths
396 of phases 1 and 2 of tremor B are different from each other. Although the
397 precision of their absolute locations are rather unreliable, different relative
398 tremor locations can be confirmed by the systematic differences in RMS
399 amplitude ratio among stations (Figs. 12, 16 and 21).

400 Let us now discuss the relationship of the estimated tremor locations and
401 the results of other geophysical observations. Aoyama and Oshima (2009)
402 reported that a step in tilt was overlapped in tremor B by the analysis of

broad-band seismograms. They interpreted that this step was caused by dike intrusions under Pon-machineshiri with its strike in the NW-SE direction with the assumption of dip of 90 degree. They estimated the top of dike should be 0.3 km above sea level to explain the tilt vector at the nearest station to the dike. Hashimoto et al. (2009) reported that total geomagnetic force significantly decreased by 2 nT at a station near the 96-1 crater after tremor B occurred. They considered that heat demagnetization occurred in association with tremor B.

Considering these results and our estimated tremor locations, we propose the following processes to the phreatic eruption on November 18 at Meakandake, referring to Fig. 22(b). There was volcanic fluid such as hot underground water and/or vapor under the NW part of Akanfuji. The activated fluid led to tremor A and high seismic activity on September 29. Such fluid was activated again on November 16, exciting tremor B. Unlike tremor A when it stayed there, the fluid moved to the the 96-1 crater, as shown by the migration of locations of phase 3 of tremor B. The fluid intruded in the form of dike with the NW-SE strike (Aoyama and Oshima, 2009), causing heat demagnetization there (Hashimoto et al., 2009). Intruded fluid caused the tremor C under the 96-1 crater on November 17, resulting in the surface

eruption on November 18. Alternatively, there are fluids already around the 96-1 crater. Tremor at source area a affects around the 96-1 crater. Tremor A caused the seismicity while tremor B affects fluids to lead the demagnetization and eruption. In this case, fluid migration was not necessary. In either case, we detected the fluid activities at source area b, which was triggered by the activities at source area a.

No significant changes found by visual observations in the 2006 craters during 2008 activity suggest that fluid were not present at that time. It was also confirmed by our analysis that no tremor location estimated around the 2006 craters. The NW end of the dike may be located around the 96-1 crater, but not extending to the 2006 craters, which restricts the geometry of intruded dike model of Aoyama and Oshima (2009). In addition, the difference in depth between phases 1 and 2 of tremor B suggests some complex mechanism of dike intrusion, and additional investigation about this intrusion mechanism will be required in the future.

8. Conclusions

We estimated the locations of tremor sequences that occurred during the 2008 activity of Meakandake volcano with the spatial distribution of seismic

amplitudes. In spite of only five seismic stations, we found the evidence of the migration of tremor locations before the eruption. The source area of tremor A on September 29 and phases 1 and 2 of tremor B on November 16 is at the NW part of Akanfuji. On the other hand, that of tremor C is around the 96-1 crater. The locations of phase 3 of tremor B appear to connect those two source areas. Although the precision of absolute tremor locations is rather low because of the limitation of station distribution, temporal variations of RMS amplitude ratios clearly show that there were two source areas between these three tremors and tremor location was clearly migrated during phase 3 of tremor B.

Considering other geophysical observations, this location migration may be related to some dynamic behaviors of volcanic fluid which caused small phreatic eruptions. In addition, a systematic difference in location depths during phases 1 and 2 of tremor B appears to reflect some complex mechanisms of dike intrusion.

Seismic observation in a volcanic area is far from an idealistic plan because of its severe environment. The distribution of seismic stations is limited in general. In addition, there are rarely precursors related to small phreatic eruptions in many cases. Our observation of the migration of tremor loca-

tions before the phreatic eruption is important in monitoring activities at Meakandake volcano, only with the limited seismic stations. Moreover, the depth migration of tremor B is important to study the fluid intrusion process. It is desired to apply the method of Battaglia and Aki (2003) or Kumagai et al. (2010) to estimate the locations of volcanic tremors in other volcanoes so that we will find new insight into both monitoring volcano activities and studying the mechanism of volcano eruptions.

Acknowledgements

The seismic network at Meakandake volcano is maintained by all the members of Volcanic Observations and Information Center, Sapporo District Meteorological Observatory. We thank to Hiroshi Aoyama for valuable discussions about the 2008 eruption of Meakandake. Comments from Akimichi Takagi, A. D. Jolly and Takeshi Nishimura improved the manuscript. We used the unified hypocenter catalogue of Japan Meteorological Agency. Digital elevation map used for contour is compiled by Geospatial Information Authority of Japan. All figures were drawn by Generic Mapping Tools (Wessel and Smith, 1991).

References

Aoyama, H., Oshima, H., 2009. Precursory activity of the 2008 eruption of Meakan-dake volcano, Programme and abstracts the Volcanological Society of Japan, P04.

Battaglia, J., Aki, K., 2003. Location of seismic events and eruptive fissures on the Piton de la Fournaise volcano using seismic amplitudes, J. Geophys. Res., 108(B8), 2364, doi:10.1029/2002JB002193.

Hashimoto, M., Nishimura, M., Arita, S., Moriyama, T., Sugawara, M., 2009. Measurement of geomagnetic total intensity on Meakandake, Chikyu Monthly, 31(12), 684-688. (In Japanese)

Ishimaru., S., Tamura, M., Hirose, W., Murayama., Y., Okazaki, N., Shibata, T., Nakagawa, M., Yoshimoto, M., Hasegawa, K., Uesawa, S., Nishimoto, J., Kosugi, A., Matsumoto, A., Baba, A., Sasaki, H., Takahashi, H., Ichiyanagi, M., Yamaguchi, T., Kohno, Y., Honda, R., Kasahara, M., Sapporo District Meteorological Observatory, Kushiro Local Meteorological Observatory, Abashiri Local Meteorological Observatory, 2009. Preliminary report on the eruption on November 2008 of Meakandake volcano, Report of the Geological Survey of Hokkaido, 80, 115-126.

(In Japanese with English figure captions)

Japan Meteorological Agency, 2005. National Catalogue of the Active Volcanoes in Japan (3rd ed.), Japan Meteorological Business Support Center, Tokyo, 635 pp. (In Japanese)

Jolly, A.D., Thompson, G., Norton, G.E., 2002. Locating pyroclastic flows on Soufriere Hills Volcano, Montserrat, West Indies, using amplitude signals from high dynamic range instruments, J. Volcano. and Geotherm. Res., 118, 299-317.

Kawakatsu, H., Yamamoto, M., 2007. Volcano Seismology, In: Kanamori, H. (Ed.), Treatise on Geophysics, Vol.4, Elsevier, pp. 389-420.

Koyanagi, S., Aki, K., Biswas, B., Mayeda, K., 1995. Inferred attenuation from site effect-corrected T phases recorded on the island of Hawaii, Pure Appl. Geophys., 144, 1-17.

Kumagai, H., Maeda, T., P. Palacious, Nakano, M., 2009. Locating volcanoseismic events using high-frequency amplitudes for volcano monitoring, Abstracts of Japan Geoscience Union Meeting, S156-001.

Kumagai, H., Nakano, M., Maeda, T., Yepes, H., Palacios, P., Ruiz, M., Ar-

511 rais, S., Vaca, M., Molina, I., Yamashina, T., 2010. Broadband seismic
512 monitoring of active volcanoes using deterministic and stochastic ap-
513 proaches, J. Geophys. Res., 115(B08303), doi:10.1029/2009JB006889.

514 Kumagai, H., Saito, T., O'Brien, G., Yamashina, T., 2011. Characterization of
515 scattered seismic wavefields simulated in heterogeneous media with to-
516 pography, J. Geophys. Res., 116(B03308), doi:10.1029/2010JB007718.

517 Phillips, S., Aki, K., 1986. Site amplification of coda waves from local earth-
518 quakes in central California, Bull. Seismo. Soc. Am., 76, 627-648.

519 Sapporo VOIC, 2008. Monthly Report on Earthquakes and Volcanoes in
520 Japan, `http://www.seisvol.kishou.go.jp/tokyo/STOCK/monthly_`
521 `v-act_doc/sapporo/2008y/105_08y.pdf` (In Japanese)

522 Ueno, H., Hatekeyama, S., Aketagawa, T., Funasaki, J., Hamada, N., 2002.
523 Improvement of hypocenter determination procedures in the Japan Me-
524 teorological Agency, Q. J. Seismo., 65, 123-134. (In Japanese)

525 Wessel, P., Smith, W. H. F., 1991. Free software helps map and display data,
526 EOS, Trans. Am. Geophys. Union, 72, 441.

527 Yamasato, H., 1997. Quantitative analysis of pyroclastic flows using infrasonic

and seismic data at Unzen Volcano, Japan, J. Phys. Earth, 45, 397-416.

Station	Factor	S.D.
V.MEAB	1.0	(none)
V.MEAA	0.738	0.228
V.MNDK	2.761	0.249
V.NSYM	1.487	0.639
V.PMNS	2.213	0.507

Table 1: Site amplification factor and its standard deviation of each stations.

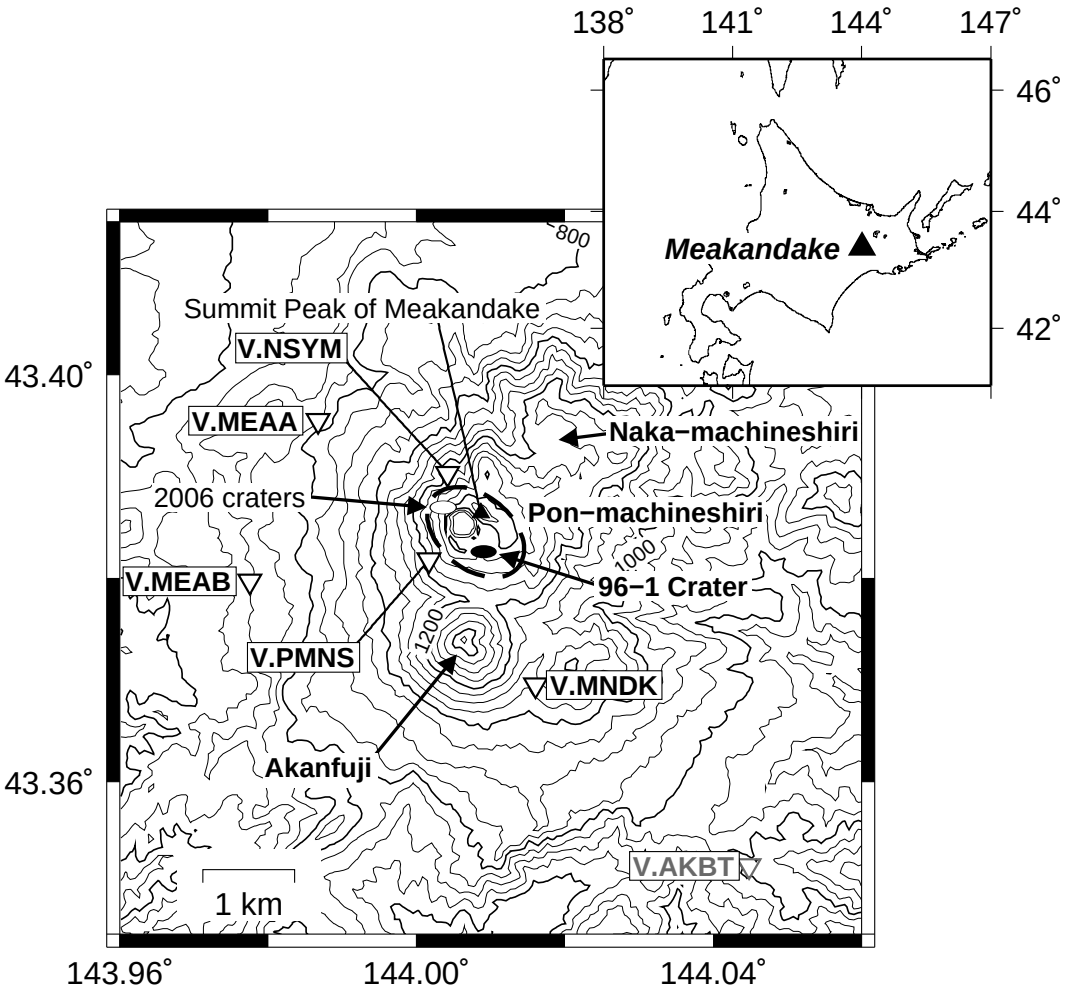

Figure 1: Locations of craters and seismic stations (inverted triangles) operated by Volcano Observation and Information Center, Sapporo District Meteorological Observatory around Meakandake volcano. Contours are plotted as each 50 m in elevation. V.AKBT in the southeast of the volcano is not used in this study.

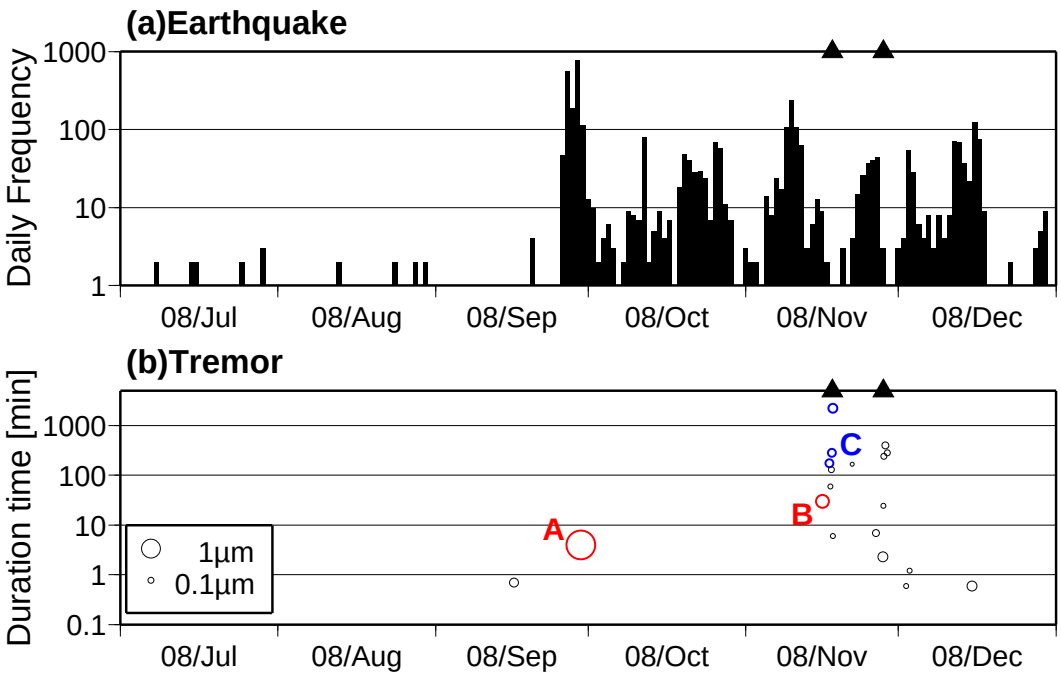

Figure 2: (a) Daily frequency of earthquakes, and (b) temporal sequence of volcanic tremors in Meakandake from July to December, 2008. Diameter of circles represents the maximum amplitude at station V.MEAB. Triangles denote the eruptions on Nov. 18 and Nov. 28. (after the compilation of Sapporo VOIC.)

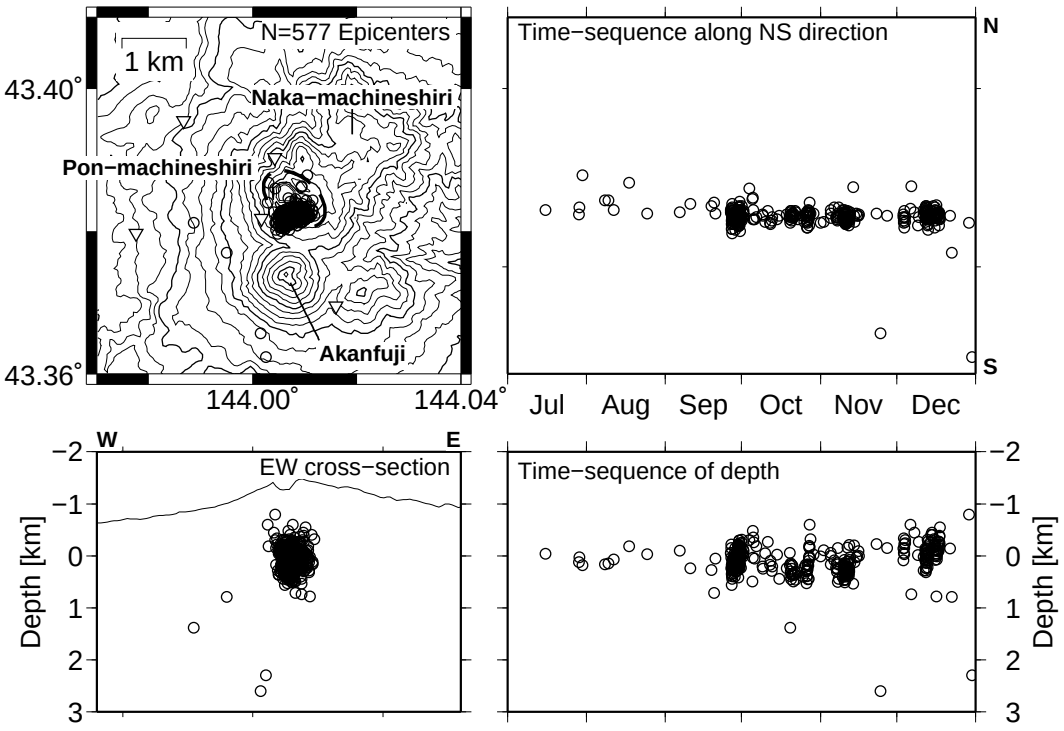

Figure 3: Hypocentral distribution from July to December 2008 at Meakandake volcano. Note that earthquakes of which hypocenters are determined are as the part of counted earthquakes (Fig. 2b).

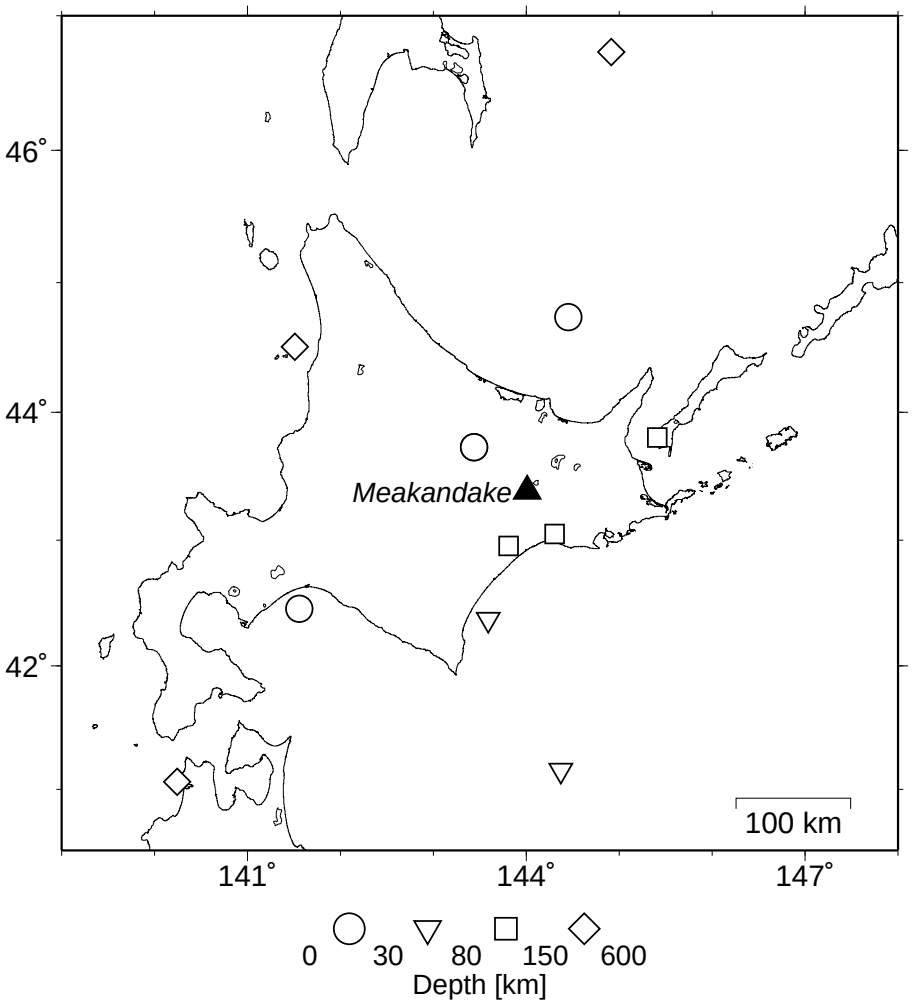

Figure 4: Hypocentral distribution used for the estimation of site amplification factors.

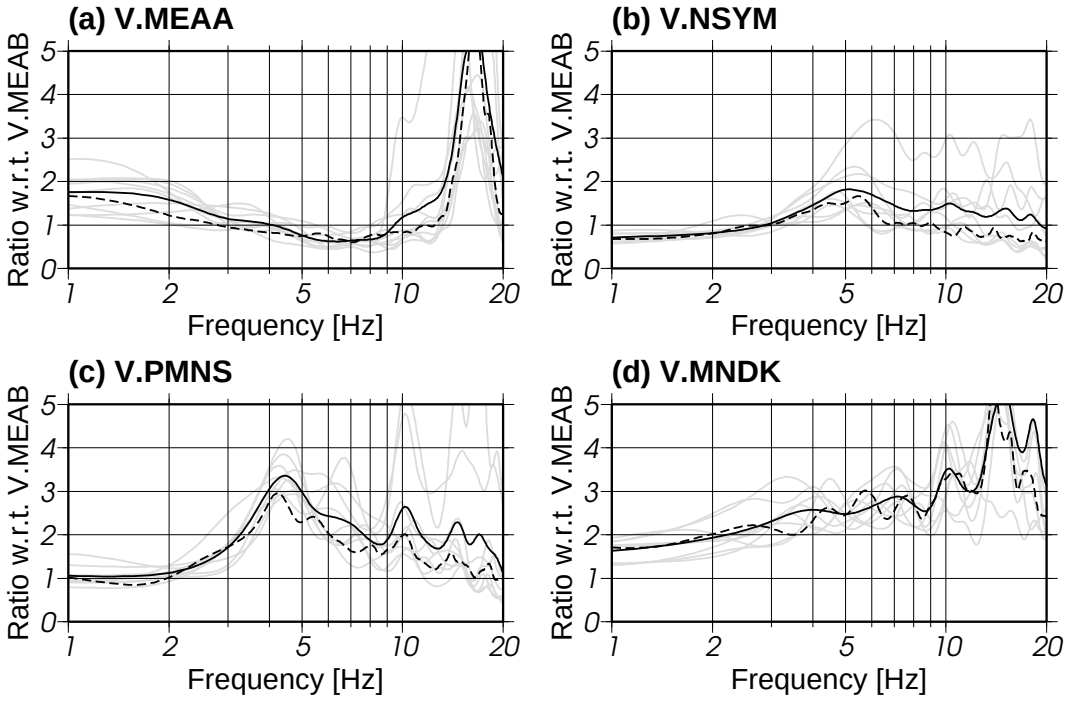

Figure 5: Spectral ratios of coda and direct S waves at four stations. All the ratios are taken with respect to V.MEAB as the reference station. Black solid lines show the averaged spectrum ratios of coda waves while gray solid lines represent the ratios of each earthquake of Fig. 4. Black broken lines show the averaged spectral ratios of direct S waves.

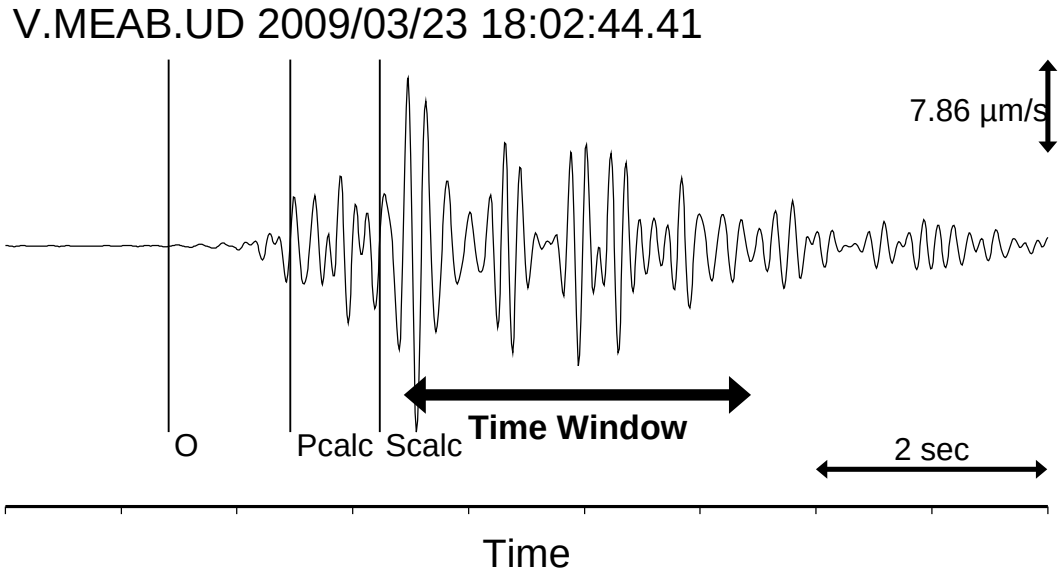

Figure 6: Bandpass filtered waveform of VT earthquake recorded at station V.MEAB on March 23. Scales of time and amplitude are shown in the right of figure. O, P_{calc} and S_{calc} mean origin time, calculated arrival time of P and S waves from the routine location.

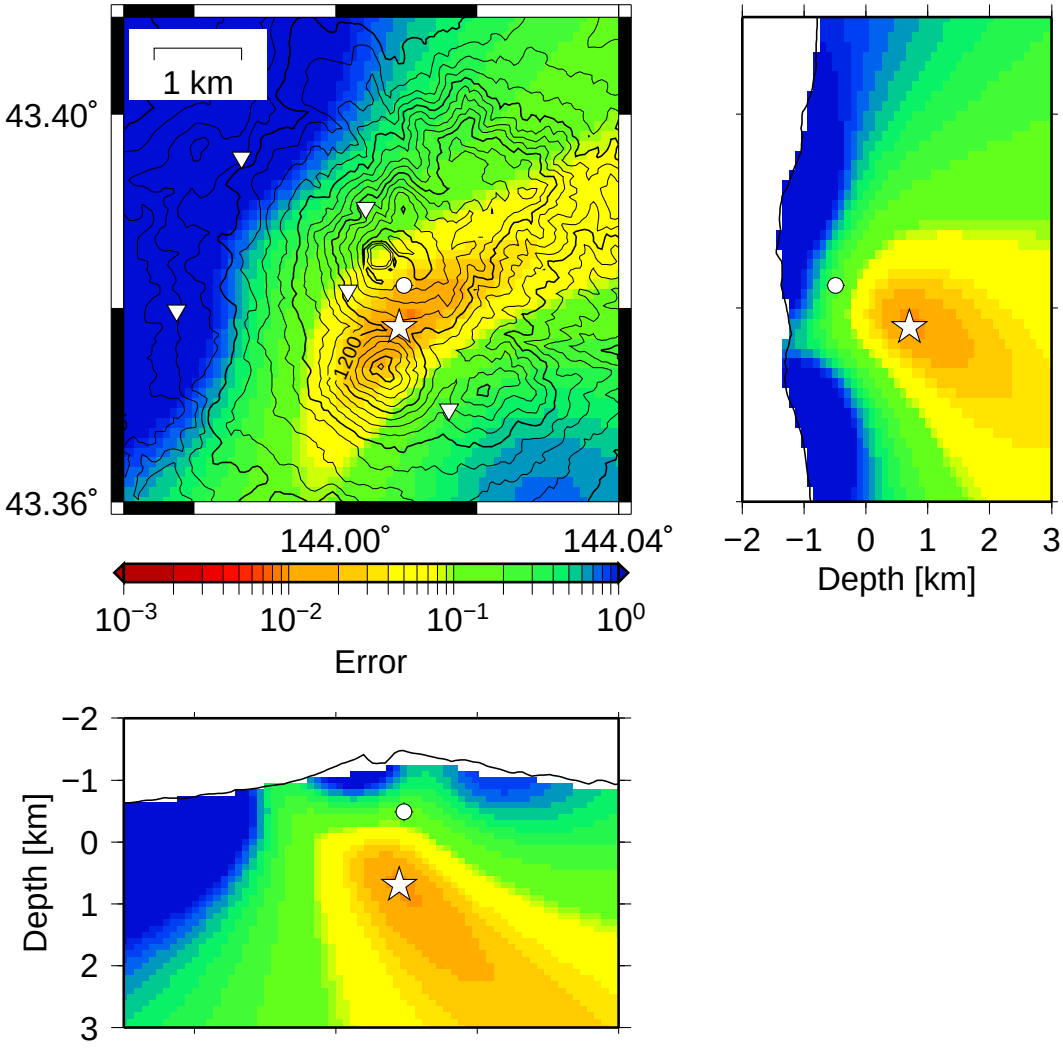

Figure 7: Estimated location (star) and routine location (circle) of the earthquake occured at 18:02 at March 23, 2009. Distribution of error are also plotted.

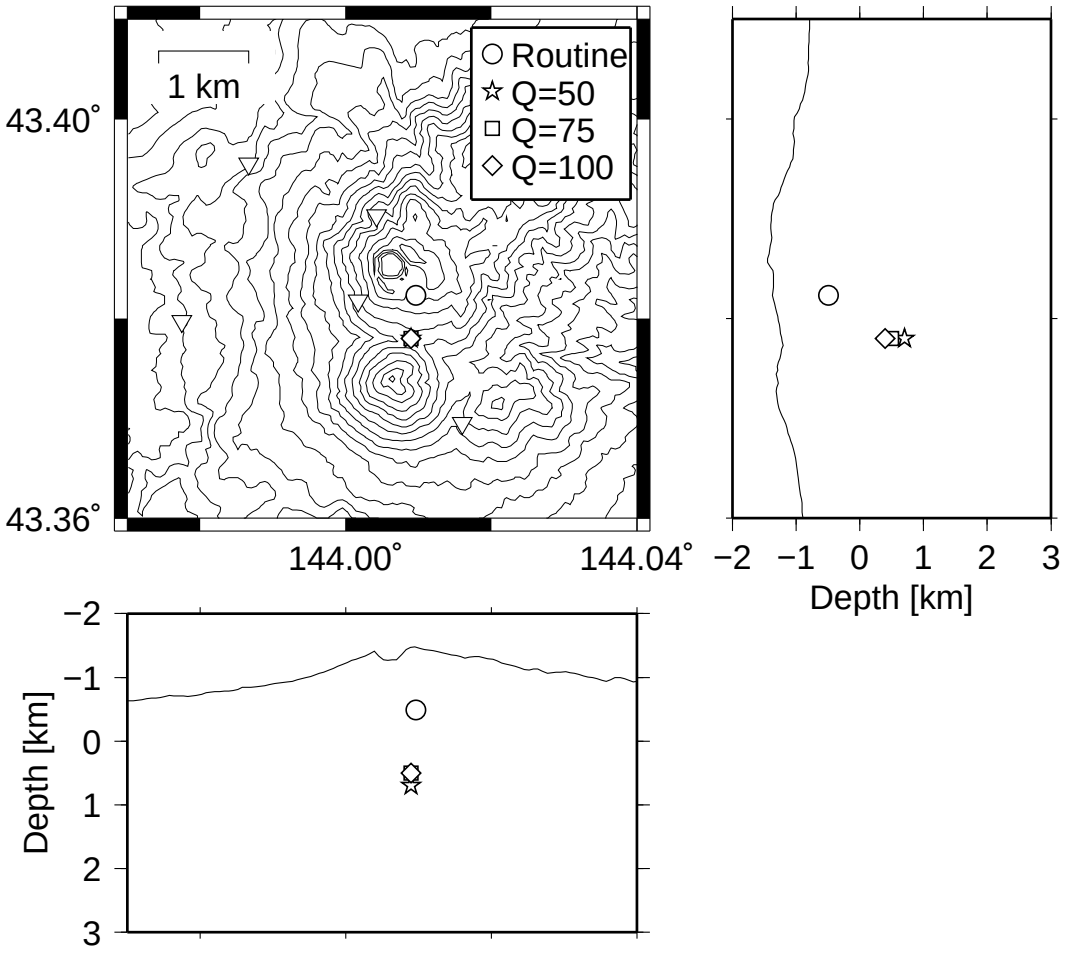

Figure 8: The result of location estimation of three Q values (50, 75 and 100) for the earthquake of Fig. 6.

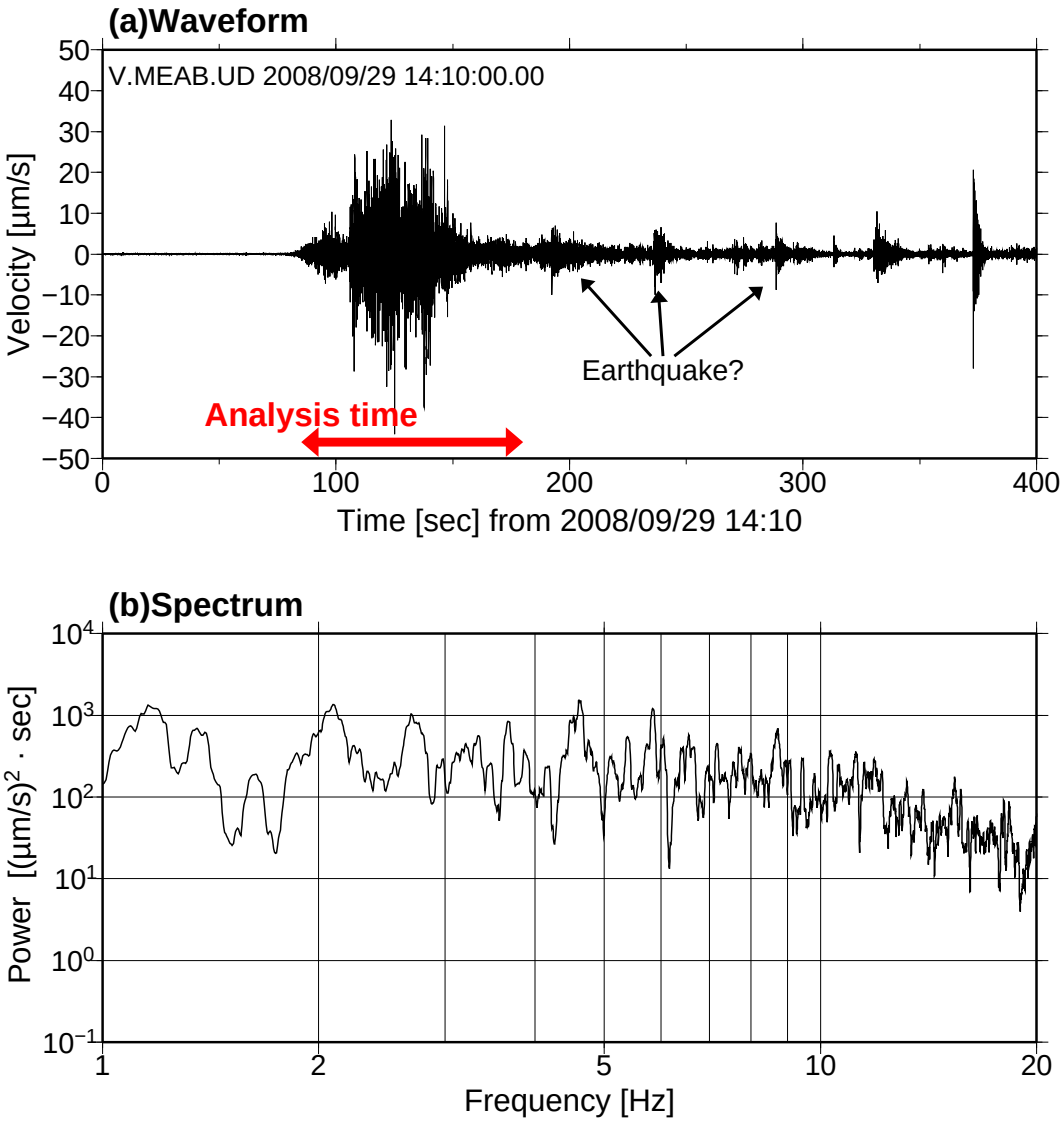

Figure 9: (a) Waveform of tremor A recorded at station V.MEAB on September 29. (b) Power spectrum of tremor A in the time window of (a) at station V.MEAB.

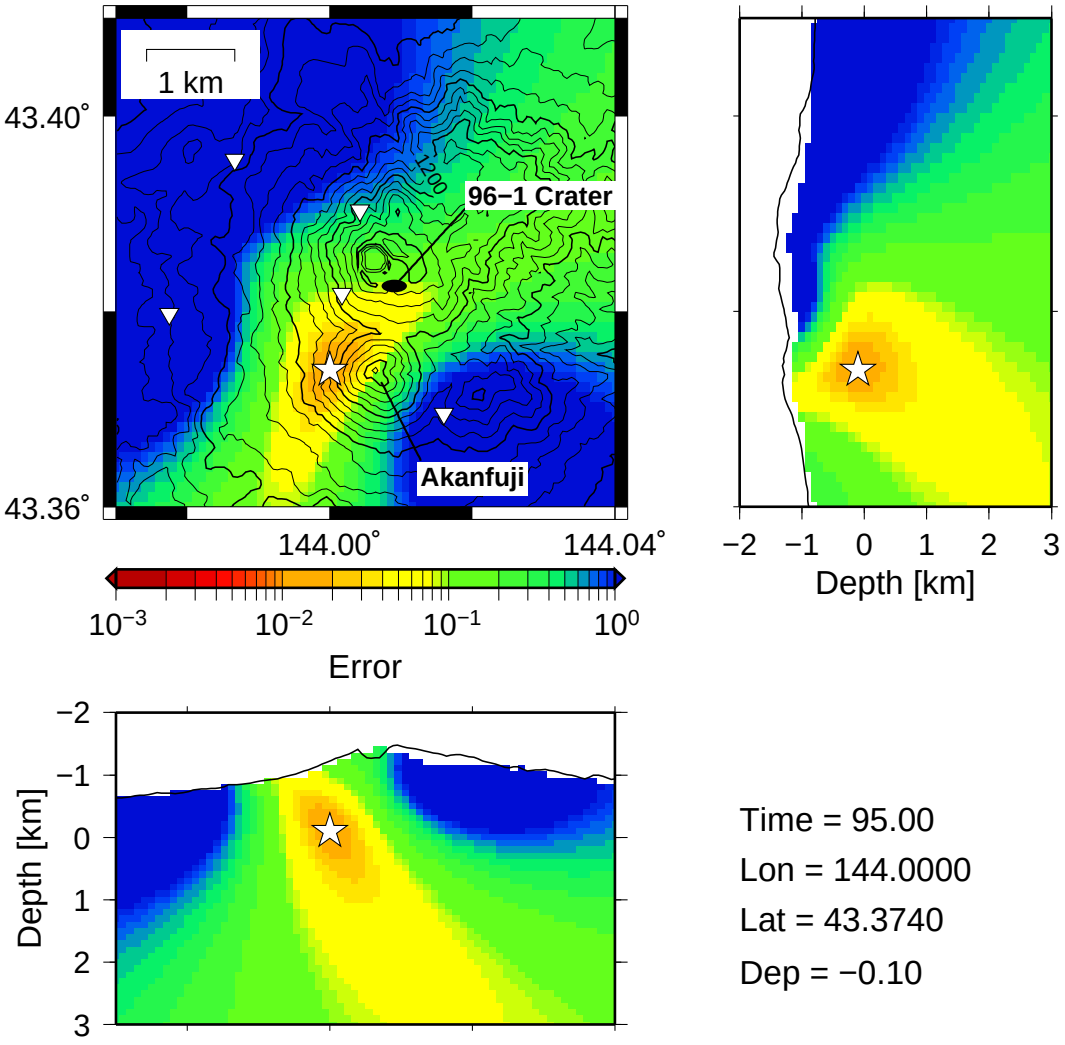

Figure 10: Spatial distribution of errors for tremor location estimation at the time window of 95 s.

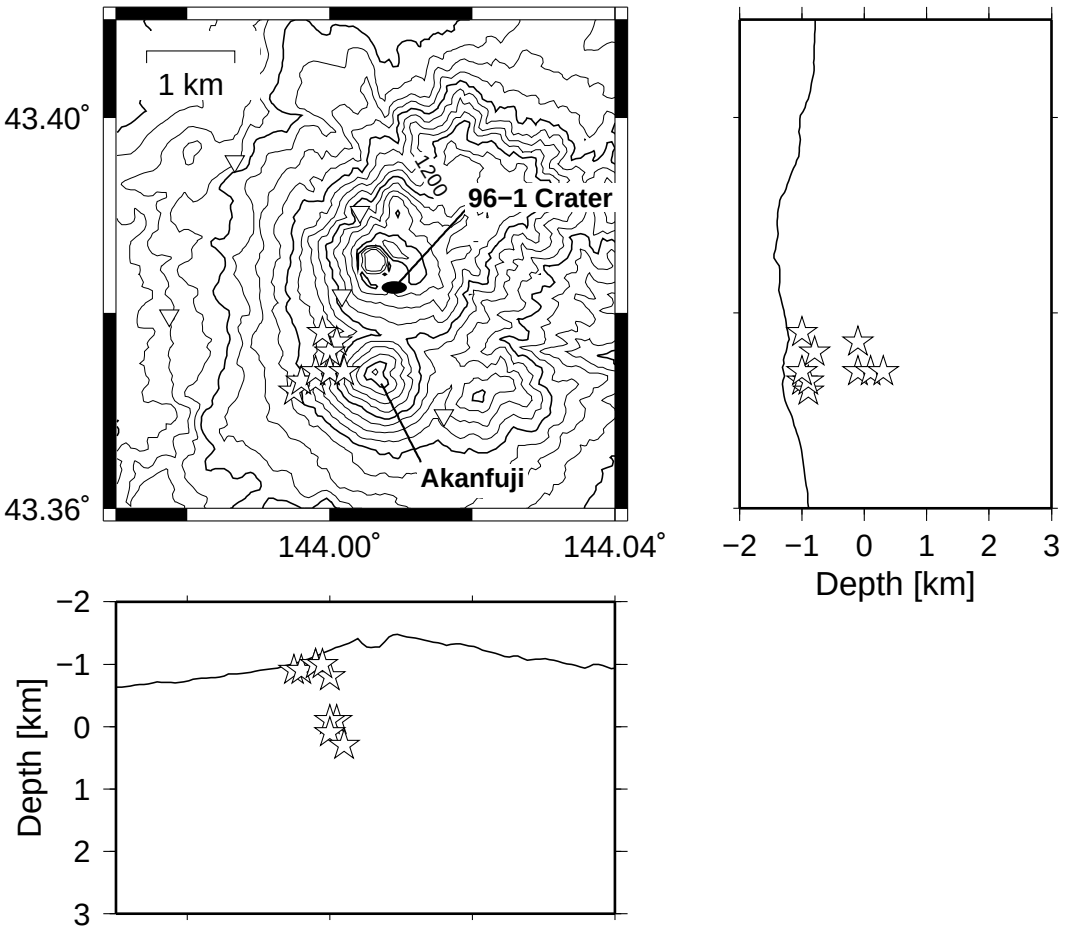

Figure 11: Estimated locations of tremor A represented by the stars. The inverted triangles represent the used seismic stations.

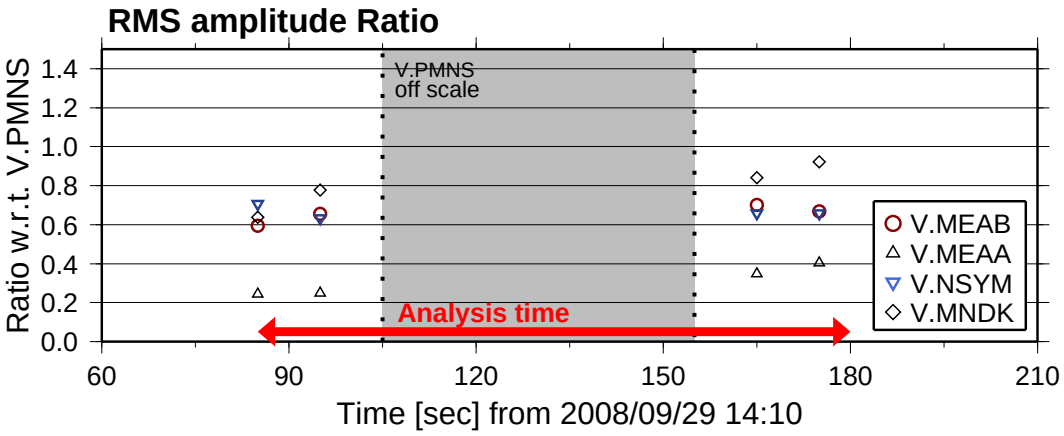

Figure 12: Temporal variation of RMS amplitude ratios of tremor A with respect to V.PMNS. The shaded area represents the time when the seismogram was scaled out at V.PMNS.

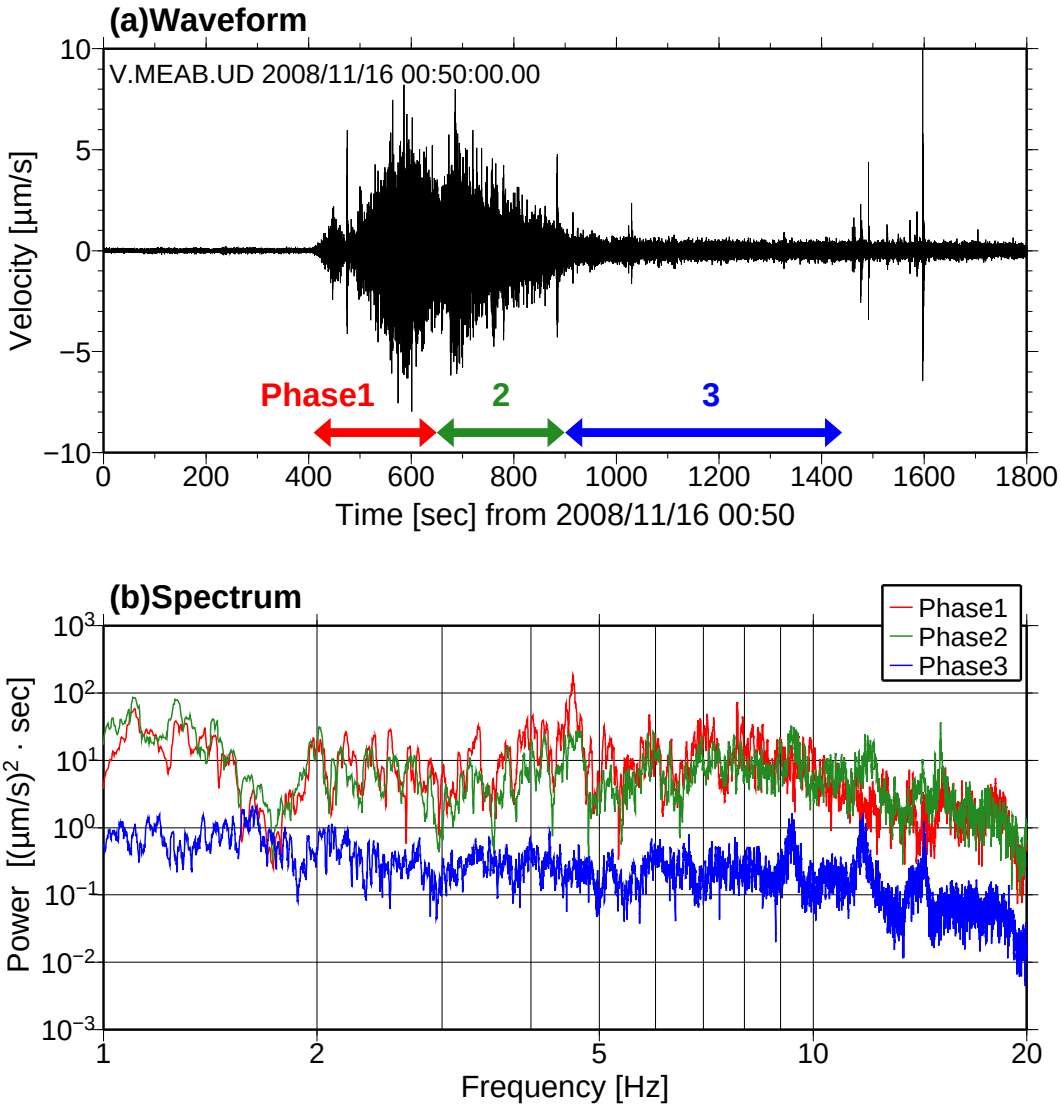

Figure 13: (a) Same as Fig. 9(a) except for tremor B on November 16. (b) Power spectrum of tremor B in the each time window of (a) at station V.MEAB.

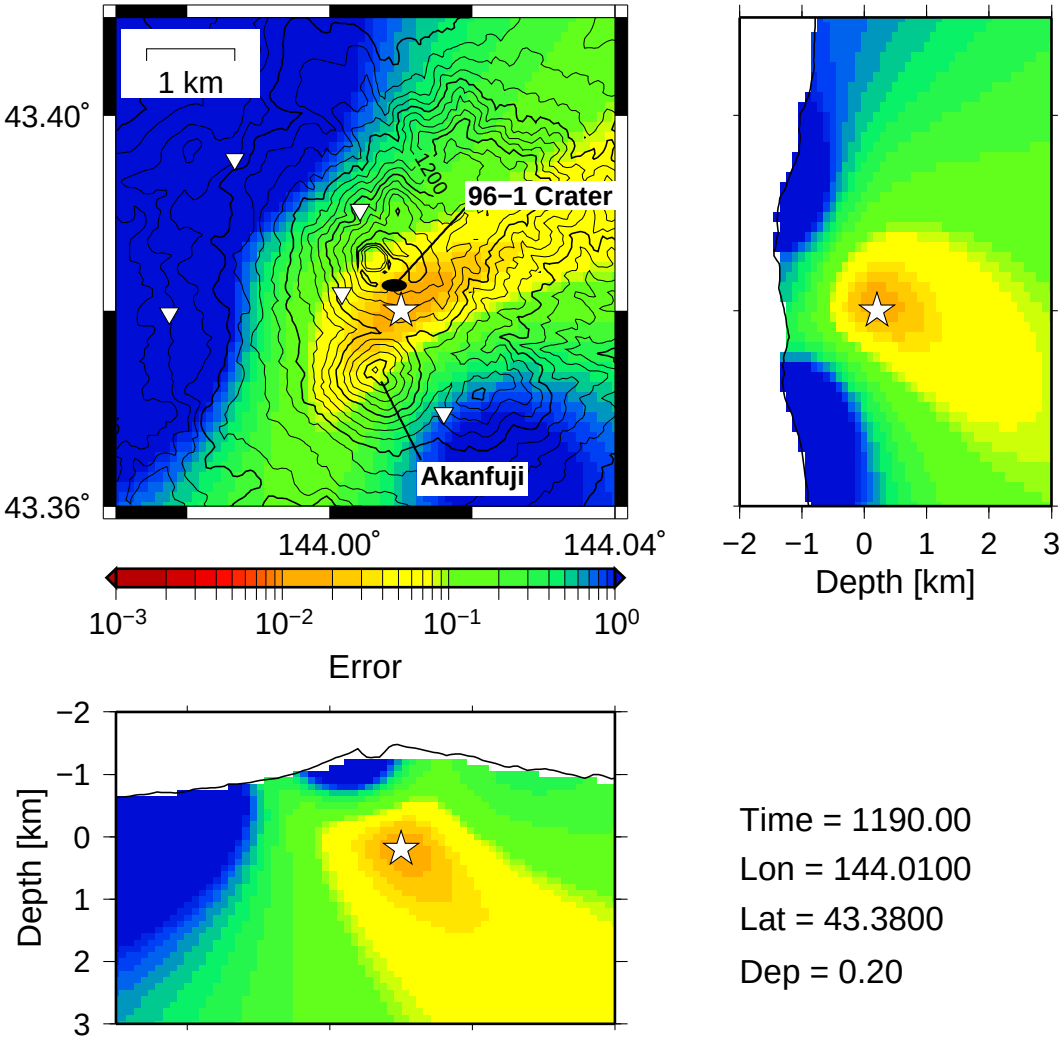

Figure 14: Same as Fig. 10 except for phase 3 at 1190 s.

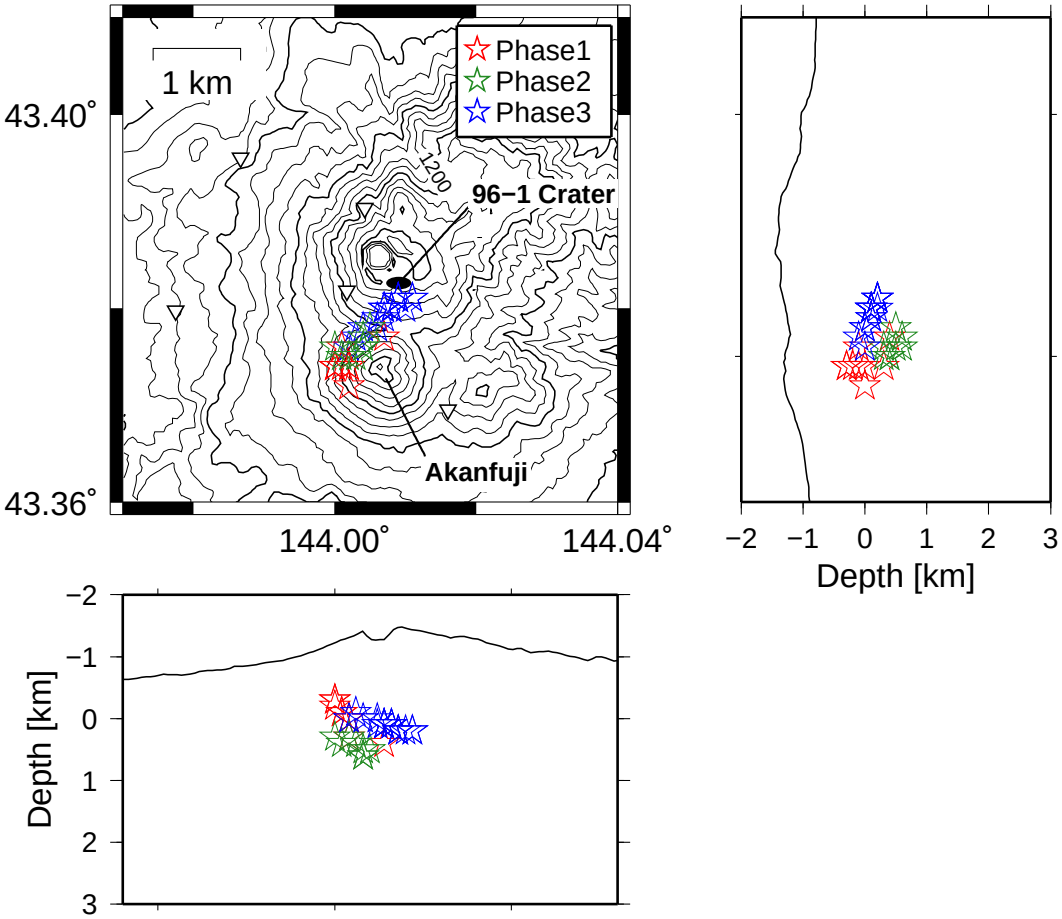

Figure 15: Estimated locations of tremor B with three phases; red stars for phase 1, green stars for phase 2, and blue stars for phase 3, respectively.

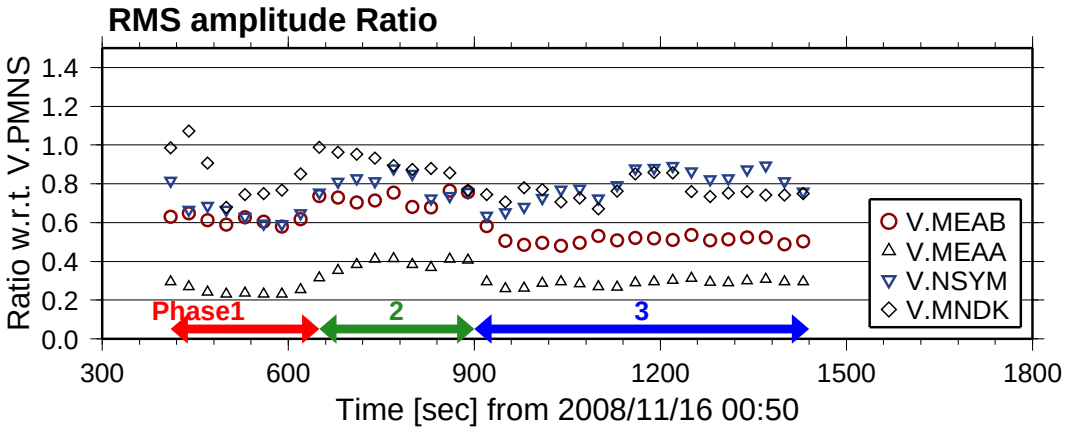

Figure 16: Temporal variation of RMS amplitude ratios during tremor B with respect to V.PMNS

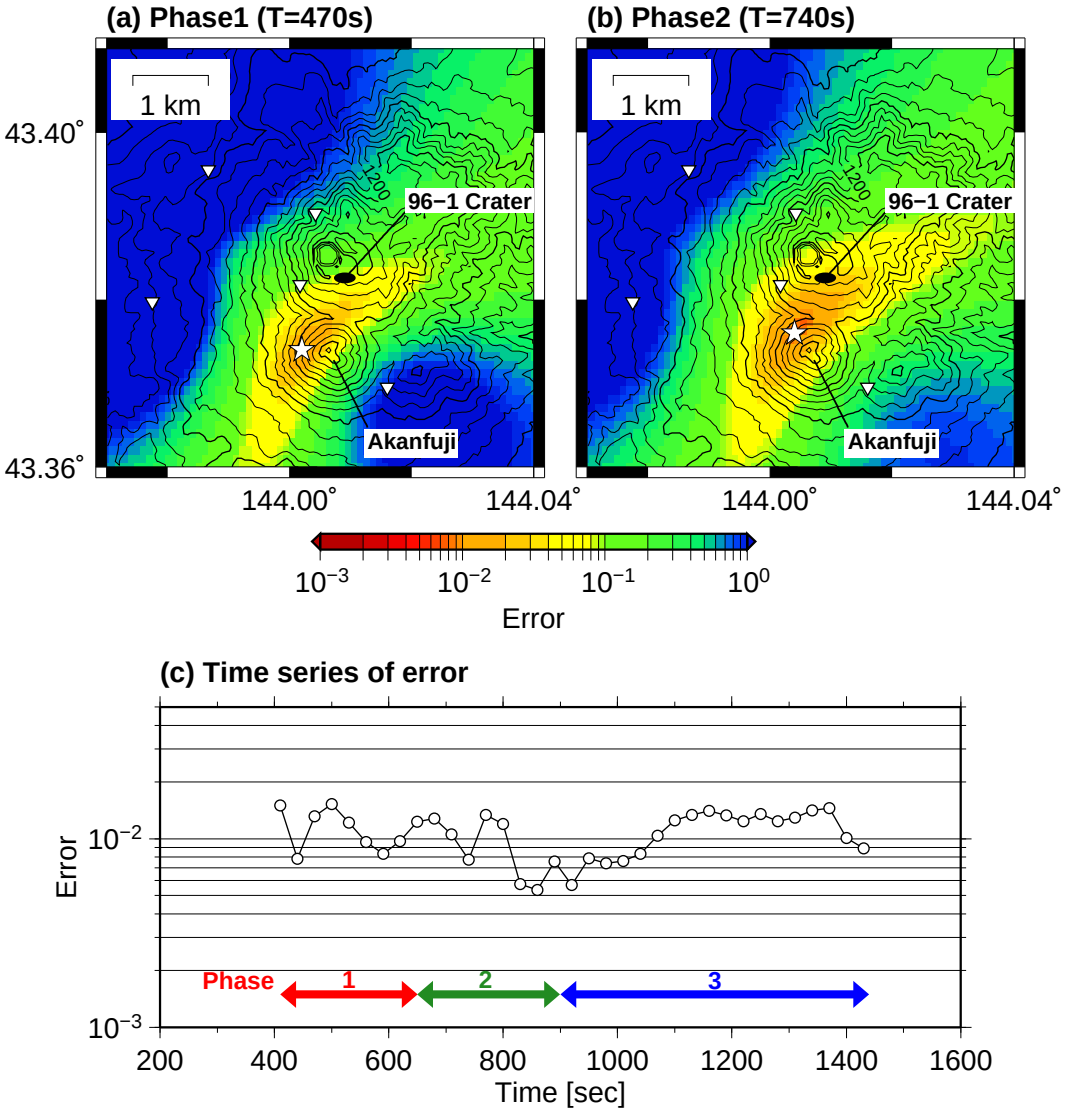

Figure 17: (a)(b) Same as Fig. 10 except for phase 1 at 470 s and phase 2 at 740 s, respectively. (c) Time series of minimum errors during the estimation of tremor B.

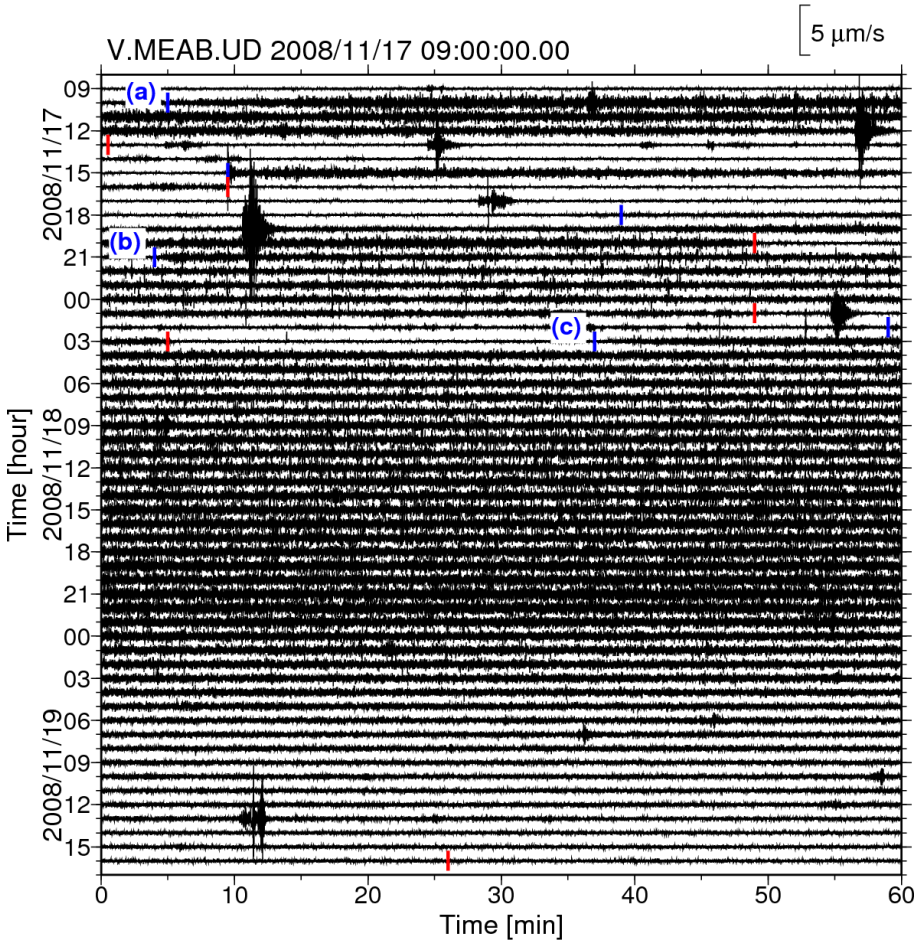

Figure 18: Continuous waveform at V.MEAB from 09:00, Nov. 17 to 16:00, Nov. 19. Start and end times of continuous tremors (after Sapporo VOIC) are denoted in blue and red lines, respectively. The labeled time windows, (a), (b) and (c), are the selected parts to estimate their locations.

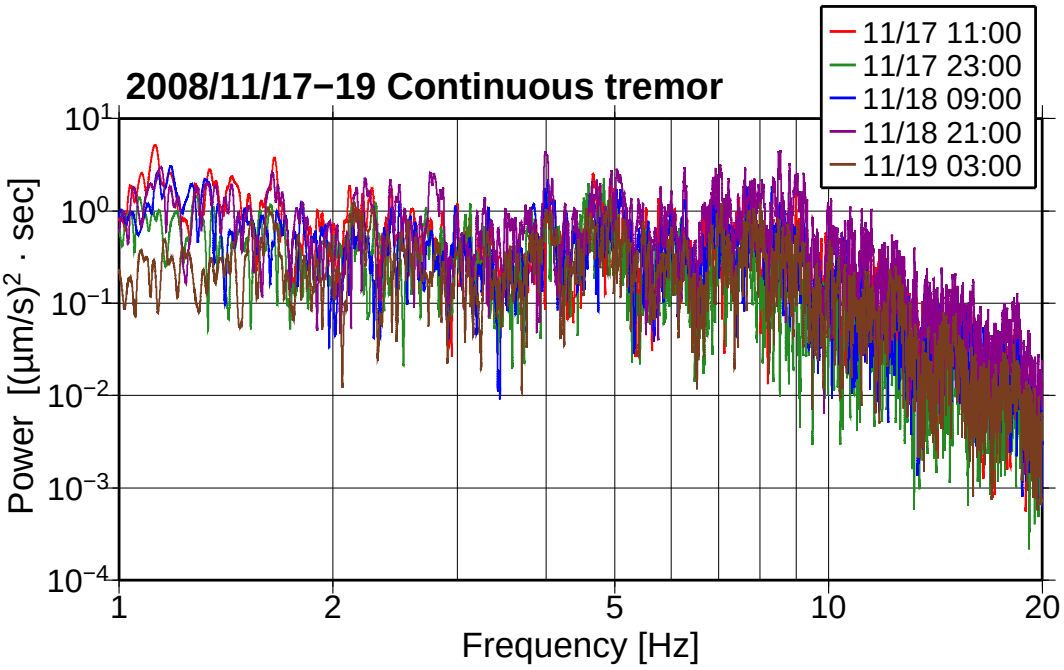

Figure 19: Power spectra of continuous tremor C at station V.MEAB. Each time window for spectral calculations is one hour.

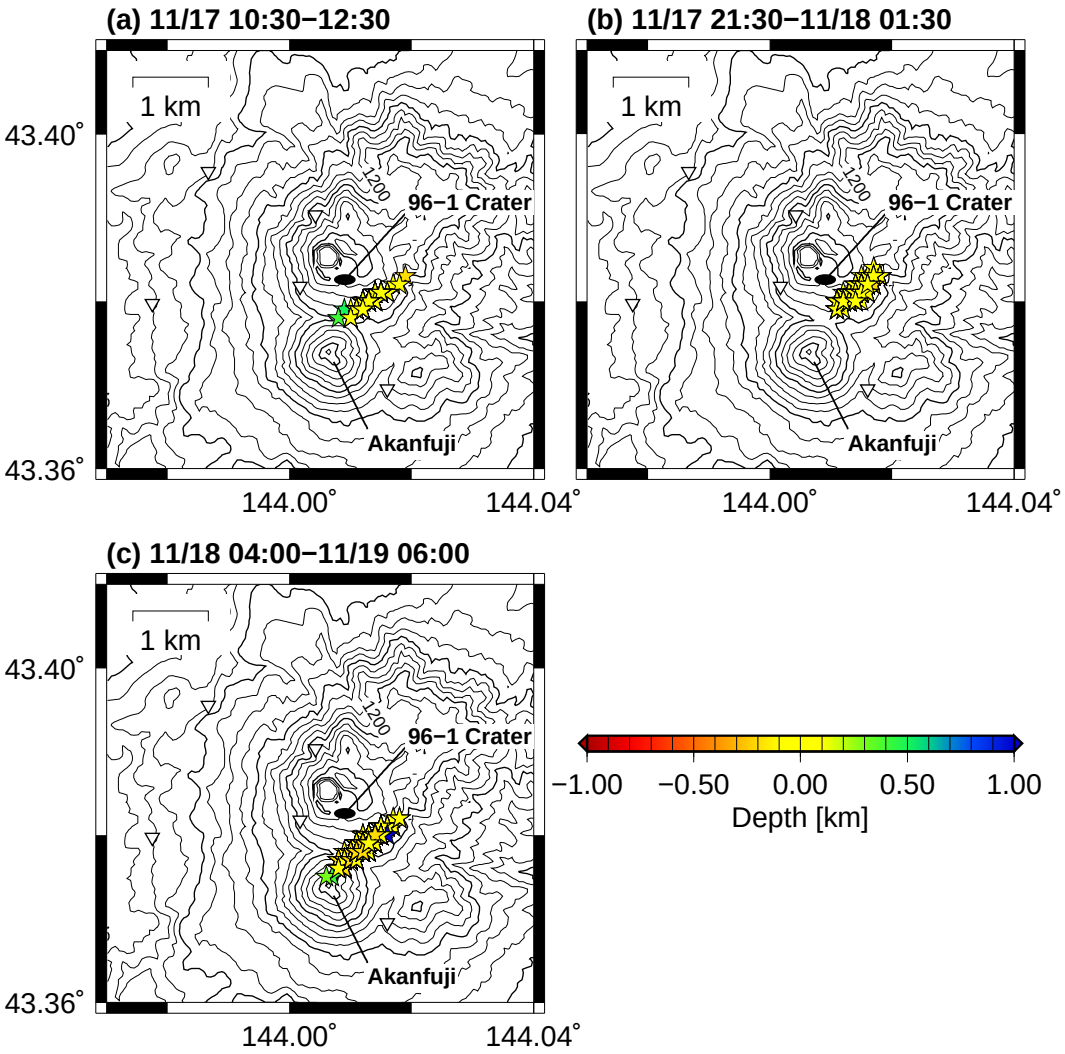

Figure 20: Estimated locations of tremor C at three times of Fig. 18.

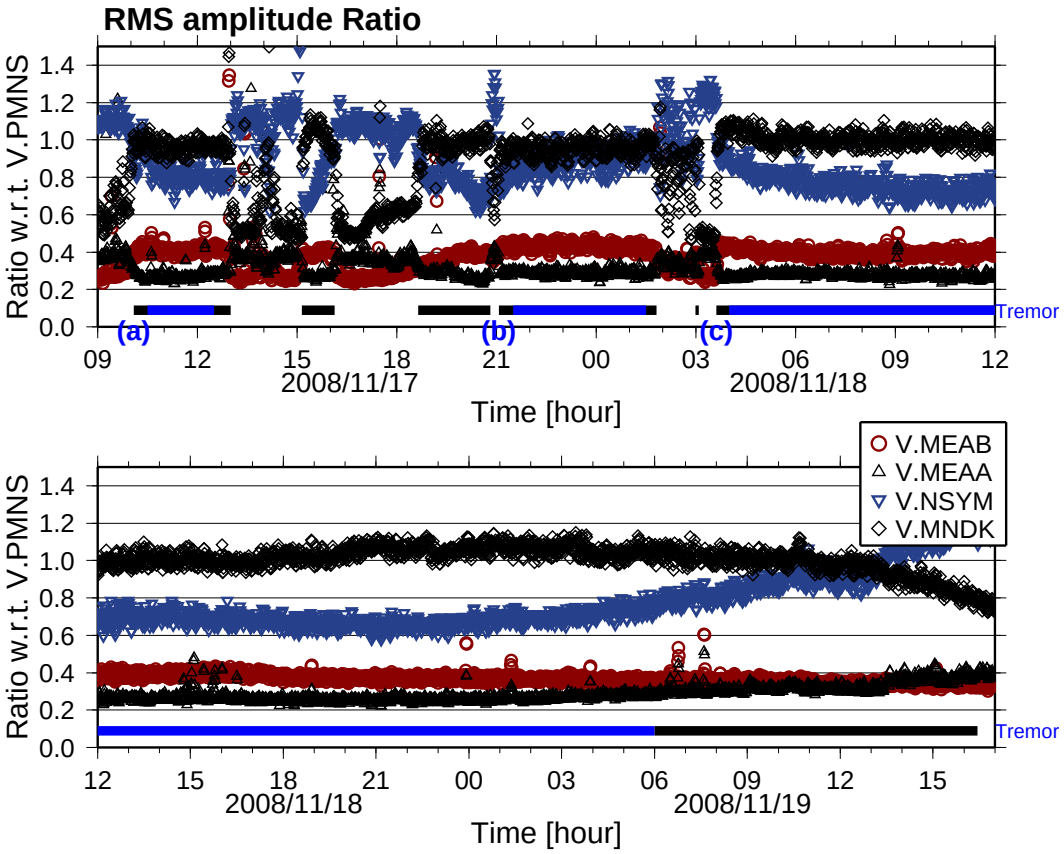

Figure 21: Temporal variation of RMS amplitude ratios of tremor C from Nov. 17 to Nov. 19 with respect to V.PMNS. The three time windows of the present analysis are shown by blue lines, other tremor sequences by black lines, respectively.

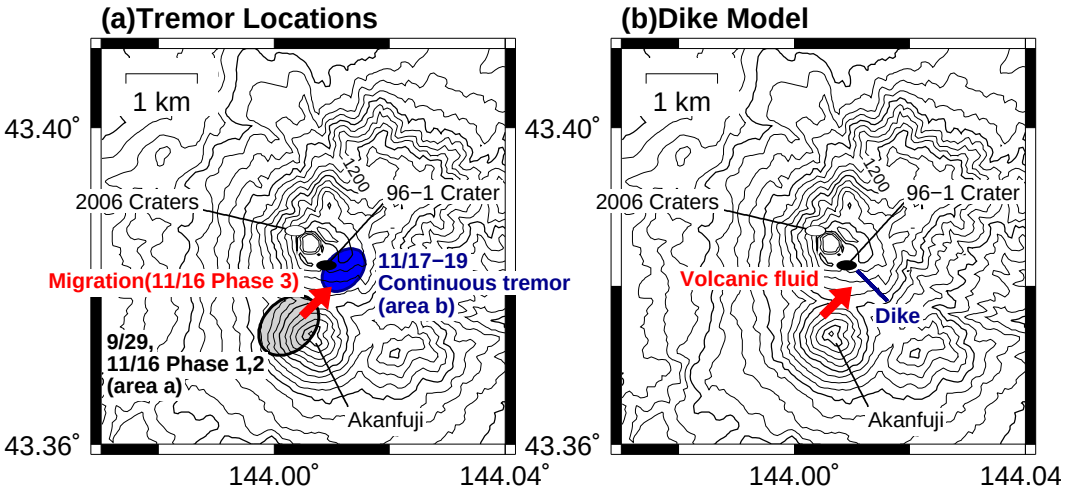

Figure 22: (a) Comparison of locations among tremor sequences. (b) A model of fluid migration and intruded dike.